Crystallisation inside fullerene related structures

Jeremy Sloan,[a,b] Jessica Cook,[a]† Malcolm L. H. Green,*[a] John L. Hutchison[b] and Reshef Tenne[c]

[a]*Inorganic Chemistry Laboratory, University of Oxford, South Parks Road, Oxford, UK OX1 3QR*
[b]*Department of Materials, University of Oxford, Parks Road, Oxford, UK OX1 3PH*
[c]*Department of Materials and Interfaces, Weizmann Institute, Rehovot 76100, Israel*

The different methods for encapsulating crystalline materials inside fullerene related structures are reviewed. The relationships between the mode of encapsulation and the crystallisation behaviour obtained in each case are described. In particular, the mechanisms of morphological and orientational control of crystallite growth inside carbon nanotubes and the comparative encapsulation behaviours of materials encapsulated by physical and catalytic methods are described and discussed. The encapsulation of defect tungsten oxide structures within inorganic fullerene-like structures are also described.

Since the discovery of carbon nanotubes in 1991,[1] a number of researchers have encapsulated both crystalline and non-crystalline materials inside their cavities using either chemical or physical methods.[2–5] Carbon encapsulation has also been achieved *in situ* by the arc-evaporation of composite carbon electrodes resulting in the formation of sealed carbon coated species contained either within the cores of carbon nanoparticles[6–12] or as continuous filling, or 'nanowires', formed along the internal bore of nanotubes.[13–15] Encapsulation has also been achieved *via* gas-phase deposition of carbon containing species onto catalytic metal particles.[16–19] In related developments, encapsulates contained within fullerene-like cage structures of the general form MX_2 (M = W, Mo; X = S, Se) have been synthesised in which the encapsulating material is grown chemically inwards from the surface of finely divided and partially reduced material.[20–25]

Encapsulation research has been directed mainly towards the enhancement of the electrical[2,6–8,13,15,25,26] and magnetic[10,27,28] properties of both the encapsulated and encapsulating materials although they are also being considered for applications in fields as diverse as biotechnology,[29] and catalysis.[4,29–32] Benefits arising from this research have so far included the ability to observe the *in situ* chemistry of encapsulated materials[33] and also size limited crystallisation behaviour on an approaching atomic scale.[11,34,35] In this article, it is the latter with which we shall be most concerned. We will attempt to elucidate some of the relationships between modes of encapsulation and the crystallisation behaviour obtained in each case. Some of the more interesting and unusual crystallisation behaviour exhibited by encapsulated species will also be described and discussed. It is hoped that these phenomena will contribute to an understanding of how materials formation can be manipulated at the most intimate scale and, additionally, how new types of materials with hybrid physical properties can be created.

Methods of encapsulating materials inside fullerene related materials

Two main strategies can be identified for encapsulating materials inside fullerene related structures. The first involves inserting the materials, either physically or chemically, into opened carbon nanotubes.[2–4] Once encapsulated, the materials can be further modified *in situ* to give reduced,[33] oxidised[34] or otherwise chemically modified encapsulates. The second strategy involves formation of the encapsulating medium around the included material. This may be achieved catalytically, either *in situ* in a carbon arc or by gas-phase deposition onto catalytic metal particles; or chemically, *via* formation of the encapsulating material from the outside surface of the encapsulated material. A third strategy can also be identified, although this is a special case restricted to the encapsulation of diamond only. Banhart and Ajayan[36] recently demonstrated that the cores of carbon onions can behave like high pressure cells in which diamond formation can be induced by irradiation with a high energy (1.25 MeV) electron beam at elevated temperatures.

Chemical insertion of materials inside carbon nanotubes

Chemical insertion involves the selective opening of the carbon nanotubes at their tips, either by refluxing in concentrated nitric acid or, alternatively, by heating in O_2[3] or CO_2,[25] and then precipitating from solution the encapsulated material inside the opened cavities. This can be achieved *via* a one-step procedure[4] in which the opening reagent contains a solubilised metal nitrate that precipitates upon calcination to form an encapsulated metal oxide. Alternatively, a two-step procedure[37] may be utilised in which the closed nanotubes are first treated with nitric acid and then heated in air to remove surface acid groups known to be present on nanotubes opened in this way.[37] The nanotubes can subsequently be filled by stirring with a solution of a metal nitrate or the metal halide, followed by calcination. This technique is useful for encapsulating materials that can interact unfavourably with surface acid groups, such as the metal halides.

Oxides of the metals Ni,[4] U,[4] Co,[4] Fe,[4] Nd,[38] Sm,[38] Eu,[38] La,[38] Ce,[38] Y[38] and Cd[38] have all been encapsulated *via* the one-step procedure. The mixed-metal oxide $FeBiO_3$ has been similarly encapsulated[38] by calcining a mixture containing an equimolar solution of iron and bismuth nitrates, concentrated HNO_3 and closed nanotubes. Pd,[37] Ag,[39] Au[39] and AuCl[39] have all been encapsulated using the two-step procedure using, in the case of the latter three, their respective metal halides. In a modification to the two-step procedure,[34] polycrystalline SnO has been encapsulated by mixing opened nanotubes with $SnCl_2$ in acidic solution to which was added a weak base, resulting in precipitation at a pH of 10.2.

† Present address: M.I.T., 77 Massachusetts Ave., Room 6-329, Cambridge, MA 02139, USA.

Encapsulated metal oxides can be reduced to their respective metals by reduction with hydrogen gas at elevated temperatures. Encapsulated Ni metal has been prepared in this fashion.[27] Similarly, hydrogen reduction of tubes filled with precipitated $KReO_4$ gives encapsulated crystallites of rhenium metal.[38] Encapsulated metal halides can be further modified *in situ* by treatment with H_2S gas at elevated temperatures to give their respective sulfides. Encapsulated CdS[38] and Au_2S_3[38] have both been prepared in this way.

Physical insertion of materials into nanotubes

Opened nanotubes can be filled *via* capillary action using either a low melting, low surface tension metal salt[30] or, alternatively, a eutectic or low melting mixture[34] of two components with a resulting surface tension lower than the threshold value of 100–200 mN m^{-1}.[30] When a single molten component is used, continuous and preferentially orientated filling of the nanotube cavities is invariably obtained, as has been observed for the oxide phases of lead,[2,3] vanadium[30] and molybdenum.[40] In the case of the latter, subsequent treatment of the nanotubes filled by MoO_3 with hydrogen at 450–500 °C causes reduction to pure and continuously orientated MoO_2 filling.[40] When a eutectic or low melting mixture of two components is employed, as in the case of UCl_4/KCl,[34] continuous polycrystalline filling is obtained. Encapsulated UCl_4 formed in this way hydrolyses slowly in air to give continuous filling with an oxidised product, $U(Cl,O)_x$.[34]

Arc encapsulation

The *in situ* arc encapsulation technique consists of packing a hollow graphite anode with an element to be encapsulated and then proceeding with the conventional Krätschmer–Huffman arc deposition experiment. During the arcing process, the tip of the anode and its contents are rendered into the vapour phase and the carbon shell then grows catalytically from the condensing species. This technique has now been applied to nearly half of the elements in the Periodic Table. All of the lanthanides, except Pm, Sm and Eu;[7,8,10–12,41–45] all the first-row transition metals;[11,44–49] the platinum group metals Ru,[19] Rh,[19] Pd,[19,50] Os,[19] Ir[19] and Pt;[19] selected other transition metals, such as Y,[6,12,45] Au,[8] Ta,[11,26] Mo,[11,45,48] W,[11,45,51] Nb,[45] Zr[45,49] and Re;[51] the main-group elements Ge,[14] Sn,[14] Pb,[14] Sb,[14] Bi,[14] S,[145] Se,[14] Te,[14,45] B,[14,45] Si[14,45] and Al;[45] and the actinides Th[52] and U[52] have all been encapsulated by the arc method, either as their respective carbides or in elemental form. With the exception of Cr, Dy, Ni and Gd, which are obtained as continuous filling inside nanotubes,[11] all of the encapsulates are obtained as single crystals encased inside carbon nanoparticles. However, a mixture of the latter type of filling with continuous filling is also observed in the case of the encapsulated metals or carbides of Gd,[10] Y[12] and Mn.[48]

Encapsulation *via* catalytic growth from solid particles

Arc encapsulation, as described above, is a very specific mode of catalytic growth that occurs during co-condensation after both the encapsulated and encapsulating materials have been rendered into the vapour phase. The type of catalytic growth described here pertains to gas-phase[53–56] carbon deposition onto catalytic particles. The carbon carrier can vary from hydrocarbon gases, such as methane[55] and acetylene,[57] to aromatics, including benzene,[58] to polymers, such as polyethylene,[59] and even more complex organic species.[60,61] Only certain metals efficiently promote carbon growth from the gas phase and these include Co,[16,18,53] Fe,[53] Ni,[53–55,57–60] Pd,[54] Pt,[54] Ti,[57] W,[57] Cu[61] or Ge.[61] In nearly all cases, the goal has been to produce either nanotubes or modified nanotubes, including single walled nanotubes (SWTs), rather than encapsulated species which are essentially a by-product. Recently, however, Dai *et al.*[61] have deliberately prepared encapsulated nanowires containing copper and germanium by pyrolysis of polycyclic aromatic hydrocarbons over finely divided copper and germanium, respectively.

Chemical encapsulation

MX_2–fullerene-like materials, with M = W or Mo and X = S or Se, consist of a network of 2H-MX_2 prisms that, in projection, resemble the graphitic network common to carbon fullerene related structures such as nanotubes (2H refers to the hexagonal symmetry, which repeats every two layers). The relationship between the two types of structures is shown schematically in Fig. 1. Like nanotubes and other fullerene derived structures, the interlinked 2H-MX_2 hexagonal networks are capable of incorporating different alternative polyhedra which, depending on the type, impart either positive or negative curvature into the structures resulting ultimately in the formation of nanotube and nanoparticle-like structures. Based on these relationships, such materials are often referred to as the inorganic fullerenes.

There are now a number of specific and general methods by which inorganic fullerenes can be prepared, including: spontaneous room temperature growth from reduced WS_3 soot;[22,23] gas-phase growth from ion beam sputtered W or Mo films;[62] pulsed laser evaporation from non-fullerenic MoS_2 films;[63,64] STM induced growth from amorphous finely divided MoS_3 particles;[65] and gas-phase growth from partially reduced Mo or W oxides.[20–24] Only in the last two cases are filled or partially filled encapsulates obtained whereas in the other instances, hollow inorganic fullerene cage structures are produced. STM induced MoS_2 growth produces encapsulates containing amorphous MoS_3 filling, while gas-phase growth from the reduced Mo and W oxides produces encapsulates with partially reduced oxide filling.

Relationships between mode of formation and crystallisation behaviour inside fullerene related structures

Control over crystallite morphology and orientation in carbon nanotubes

The behaviour of crystalline materials formed by precipitation inside carbon nanotubes allows for the study of their morphological control over crystallite formation. Initially, crystallisation will proceed according to conventional nucleation and growth mechanisms but once the size of the encapsulated crystallite approaches that of the internal diameter of the

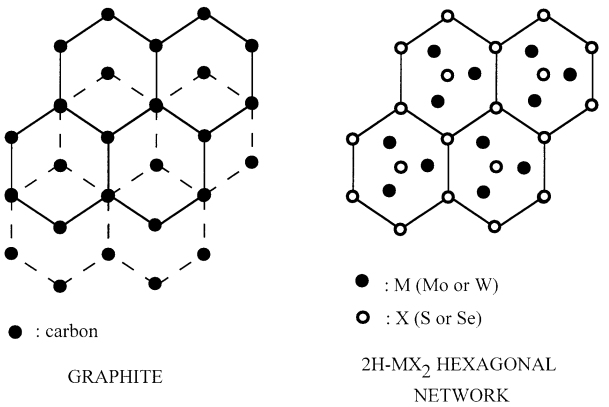

Fig. 1 Structural relationship between graphite and 2H-MX_2 structures. In both cases, the fullerene derived structures form networks of interlinked hexagonal units which can form positive or negative curvature based on the number and type of incorporated polyhedra other than hexagons.

nanotube cavity, then the walls will start to exert control over any future growth. The precise nature of the control at this juncture raises some interesting questions. How the capillary walls influence the orientational behaviour of growing crystallites and, secondly, how they interact at the atomic level with encapsulated crystalline materials are problems that are worthy of investigation.

Polycrystalline SnO forms spherical or ellipsoidal encapsulates with diameters in the range 20–60 Å[35] inside carbon nanotubes with internal diameters in the range 20–90 Å. The packing of such crystallites in nanotubes provides some direct insight into the mechanisms of control over crystallisation. Fig. 2(a) shows a high-resolution transmission electron micrograph (HRTEM) of an agglomeration of randomly orientated SnO crystallites inside a nanotube with a large internal diameter (*ca.* 90 Å). In this instance, the nanotube exerts morphological control over the agglomeration but not over the individual crystallites. In Fig. 2(b), another micrograph showing a nanotube with a smaller diameter (*ca.* 35 Å) can be seen in which two well resolved and slightly elongated crystallites **I** and **II** reside in the central cavity. A third, less well resolved crystallite (**III**) is also visible. Whereas crystallite **I** has its growth axis (arrowed) aligned parallel to the nanotube axis, crystallite **III** has effectively two growth axes (arrowed) that are both at an angle to the tube axis. Regardless of where the nucleation of crystallite **II** started, the crystal growth in either of the two directions must come to an end once it meets the carbon walls. By contrast, crystallite **I** may continue growing along its current axis until either it meets an obstruction or until the crystallisation process is terminated. In Fig. 2(c) a micrograph of a nanotube with a more regular packing of SnO crystallites can be seen.[35] In this case the smaller crystallites observe apparently random orientations while the larger crystallites (denoted **IV**), all have their d_{101} lattice fringes orientated at 90° with respect to the nanotube wall. The nanotubes capillaries shown in Fig. 2(b) and (c) clearly exert influence over both the morphology and orientation of their encapsulated SnO crystallites. The type of morphological control exhibited by SnO can sometimes lead to some interesting behaviour inside the capillaries of carbon nanotubes. Fig. 3(a) and (b) show a micrograph and schematic representation of a crystal spiral formed from a chain of single SnO crystallites of approximately equal size and observed to form inside the capillary of a carbon nanotube.[35] The mode of formation of such a spiral can be explained completely in terms of the mechanisms of morphological control described above.

Other examples of polycrystalline filling show similar types of morphological and orientational control to SnO. Fig. 4(a) and (b) show examples of filling with polycrystalline SnO_2[66] and ZrO_2,[66] respectively. Whereas polycrystalline SnO forms small crystallites with diameters approximately equal to the internal diameter and which apparently randomly orientate along the nanotube capillary, polycrystalline ZrO_2 crystallites

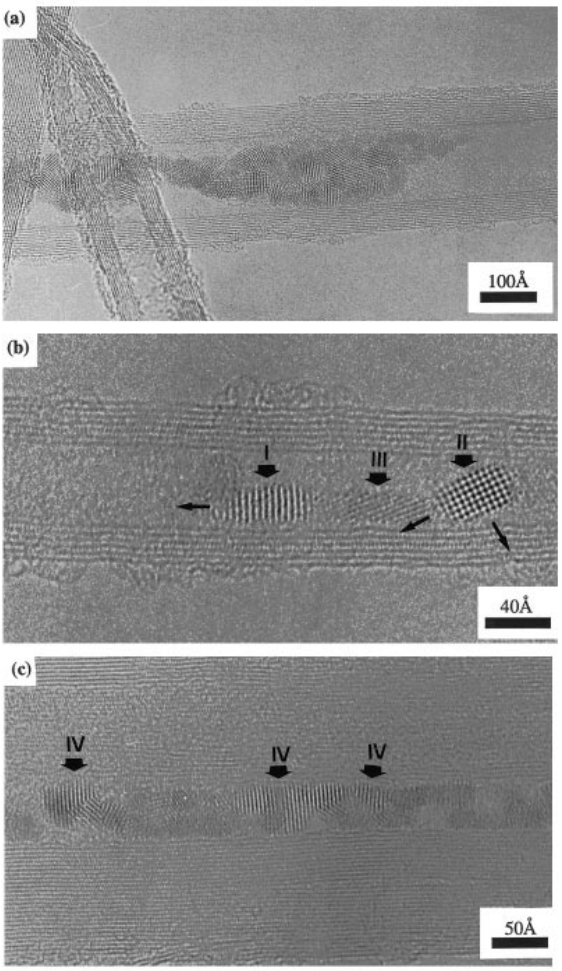

Fig. 2 (a) Micrograph illustrating nanotube capillary morphological control over agglomerated SnO crystallites. The crystallites clump together and effectively form a blockage inside the capillary. (b) Micrograph showing orientational control over individual crystallites. **I** is free to grow along its crystallite axis while the growth of **II** is constrained by the nanotube capillary. (c) Random and preferentially orientated SnO crystallites (**IV**) inside a densely packed carbon nanotube.

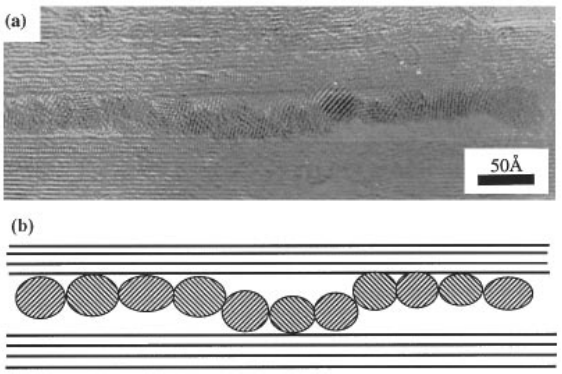

Fig. 3 (a) Spiralling crystal growth, induced by morphological control, observed inside a carbon nanotube capillary. (b) Schematic representation of spiralling crystal growth.

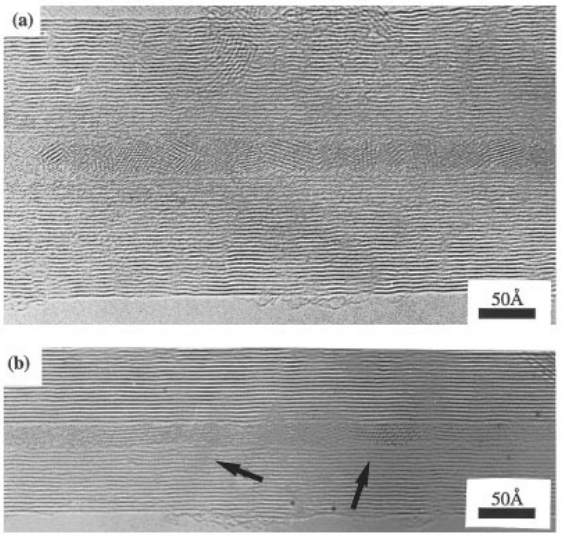

Fig. 4 (a) Randomly orientated SnO_2 crystallites observed inside a nanotube capillary. (b) Preferentially orientated ZrO_2 crystallites (arrowed) observed inside a nanotube capillary.

are elongated and several are aligned with their lattice fringes parallel to the nanotube axis.

In order to attempt to answer the question of how crystalline materials interact with carbon nanotube walls, it is instructive to look at well resolved HRTEM images of continuous crystalline filling. Fig. 5(a) shows an elongated Sm_2O_3 crystallite, that completely fills the internal volume of a nanotube for a distance of *ca.* 600 Å. Beneath this image are two enlargements [Fig. 5(b) and (c)] of regions at intervals along the capillary where the image contrast reveals the same precise arrangement of the Sm^{3+} cations (which image much more strongly than O^{2-} and resolve as dots) at the interface of the Sm_2O_3 crystallite with the nanotube wall. The cations closest to the nanotube wall can be seen to be arranged in a triangular motif that extends along the wall of the carbon nanotube. Due to a slight tilt in the crystal, the lattice image in Fig. 5(b) images more strongly as lines which actually represent the (400) planes of Sm_2O_3, although the motif is still just visible. This motif actually represents the point at which parallel Sm_2O_3 (222) lattice planes terminate along the nanotube wall and this occurs at precise intervals of 5.46 Å (equivalent to d_{200} of Sm_2O_3). The precise arrangement is depicted schematically in Fig. 5(d). If we now look at a two-dimensional projection of a carbon nanotube wall [Fig. 5(e)], we see that the unit cell of hexagonal graphite repeats every 2.13 Å along the axis of the carbon nanotube. This is incommensurate with the periodicity of the (222) lattice plane terminations [shown schematically in Fig. 5(d)]. Thus, in the case of this Sm_2O_3 crystallite, the orientation and periodical arrangement must be a function of the gross morphological influence of the nanotube capillary during crystallisation rather than any influence due to the atomic arrangement of the nanotube wall.

When materials are inserted into nanotubes by capillary action, the orientational behaviour of the encapsulated crystalline material is much the same as described above. As Ajayan *et al.*[30] have noted for V_2O_5 and Chen *et al.*[40] have similarly noted for MoO_3, continuously orientated behaviour is almost invariably obtained. The one exception to this is when the filling is achieved using a low melting mixture. In the case of UCl_4/KCl, continuous polycrystalline filling is obtained. Fig. 6(a) shows an example of continuously orientated MoO_3 filling. The spacing of the observed lattice fringes is 3.7 Å, which corresponds to the *c* lattice repeat of MoO_3.[40] This distance is also incommensurate with the atomic periodicity of the carbon nanotube wall along the tube axis (2.3 Å). Hence crystal growth along the nanotube in this instance is again a function of orientational and morphological control. Fig. 6(b) shows an example of polycrystalline filling obtained inside nanotubes filled using a low melting mixture.[34] The filling in this case is polycrystalline with several crystallites (denoted **V** in the micrograph) apparently observing the same preferred orientation, analogously to the case of SnO and ZrO_2, described above.

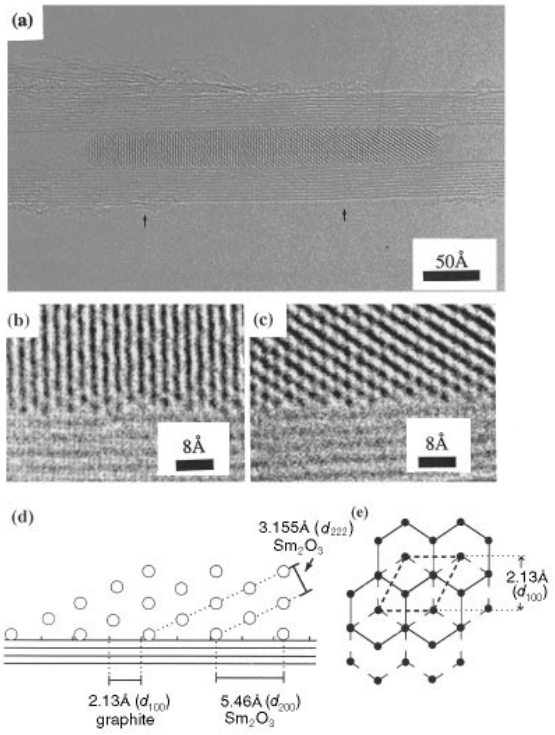

Fig. 5 (a) 600 Å long Sm_2O_3 crystallites observed inside the bore of a carbon nanotube. (b), (c) Enlargements of Sm_2O_3/carbon interface showing periodic stacking of Sm^{3+} cations. (d) Schematic representation of termination of Sm_2O_3 (222) lattice planes on carbon wall. (e) Schematic projection of graphitic nanotube wall showing periodicity of graphitic network (repeats every 2.3 Å). This is incommensurate with the repeat of (222) lattice plane terminations.

Formation of products inside catalytically formed carbon cages

There is still much uncertainty concerning the mechanism of formation of materials encapsulated by the arc method. Giuerret-Piécort *et al.*[11] claim that the propensity for the formation of long metallic 'nanowires' rather than encapsulates inside nanocapsules is correlated with the existence of an incomplete shell in the most stable ionic state of the element. Saito *et al.*[67] have indicated that there is an additional correlation for lanthanoids between their volatility and their ability to form encapsulates. Recently however, Seraphin *et al.*[45] have indicated that neither of these models are wholly without exceptions and have advanced their own model, defined in terms of the interfacial compatibility of the carbide with the encapsulating graphitic network. The phenomenon of arc encapsulation is further complicated by the fact that, in some cases, mixed products are often obtained. In the case of encapsulated manganese, for example, Liu and Cowley[47] have observed no fewer than four different encapsulated carbides, Mn_3C, Mn_5C_2, Mn_7C_3 and $Mn_{23}C_6$, some of which are incommensurate and presumably metastable. Similarly Sloan *et al.*[51] have observed the formation of rhenium metal, hexagonal ReC and an unknown metastable Re_xC_y product inside carbon nanocapsules. A micrograph obtained from the latter

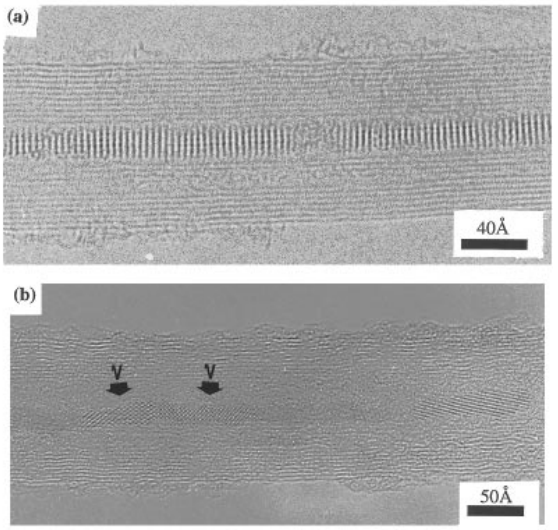

Fig. 6 (a) Micrograph showing continuous MoO_3 filling formed by the capillary method. The lattice fringes repeat at regular intervals of 3.7 Å which is incompatible with the repeat of the graphitic network (2.3 Å; see Fig. 5). (b) Polycrystalline UCl_4 arranged along the bore of a carbon nanotube obtained *via* eutectic filling. Some crystals show clear preferred orientations (**V**).

product is reproduced here [Fig. 7(a)]. Giuerret-Piécort *et al.*[11] have observed the formation of both microcrystalline Yb and 'spiral' Dy products in their nanowires, both of which are also indicative of a complex formation process. In view of the complexity of the products obtained in these and other cases cited in this article, it seems unlikely that one model or explanation alone will suffice to account for all of the encapsulation behaviour observed in arc deposited products. A particular practical difficulty is the fact that there is at present no effective way of observing *in situ* the encapsulation process. Perhaps a better approach is to consider each case individually, taking into consideration the complex kinetic and thermodynamic mechanisms that can be obtained within a particular system.

The natures of the encapsulated products obtained in the case of gas-phase deposition onto catalytic particles are much simpler to interpret than those of species formed by arc co-deposition. In general, encapsulation has been proposed to proceed *via* a solution–precipitation mechanism,[56,68] which involves absorption of carbon onto the surface of the catalytic particle resulting in the formation of a small amount of interfacial carbide, thus leaving the remainder of the encapsulate in its native elemental state. The carbon then grows progressively from the element/carbide interface. An example of an encapsulated Ni particle formed in the presence of a Ni-Harshaw catalyst at 780 °C, according to conditions specified by Tsang *et al.*,[55] is shown in Fig. 7(b).

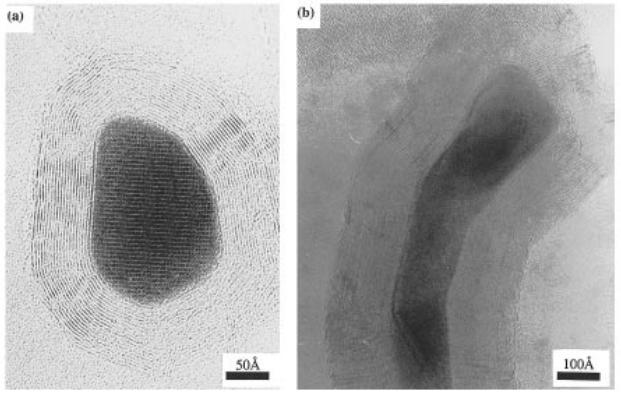

Fig. 7 (a) Microstructure of the encapsulated metastable Re_xC_y product formed *via* arc co-deposition. (b) Micrograph showing Ni encapsulated by catalytic formation of carbon from the Ni-Harshaw catalyst.

Novel layered and defect structures observed inside inorganic fullerenes

The encapsulation mechanism of sulfide and oxide particles encapsulated inside inorganic fullerenes is relatively easy to interpret for the simple reason that the encapsulating material is formed by consumption of the outside of the encapsulated material. Thus, the growth mechanisms can be interpreted in terms of progressive growth from the exterior. The three different mechanisms for STM induced MoS_2 growth from MoS_3, gas-phase growth of MoS_2 from condensing MoO_{3-d} vapour and gas-phase reaction with solid WO_{3-d} are depicted schematically in Fig. 8(a), (b) and (c), respectively.

In the case of MoS_2 induced growth in the STM, encapsulation results in the formation of amorphous MoS_3 encapsulates only. In this instance, the morphology of the resulting encapsulates will be influenced by the morphology of the amorphous precursors. In the case of the formation of Mo and W oxide encapsulates, the first occurs wholly in the gas phase whereas the second occurs as a gas–solid reaction with the oxide remaining in the solid phase. The encapsulation mechanism of MoO_{3-d} will presumably be similar to that exhibited by arc deposited encapsulates (see above), with the whole process occurring during condensation from the vapour phase. The morphology of the encapsulated products will therefore be determined by the extent of reaction and the conditions of condensation. Feldman and coworkers[24,69] have observed a

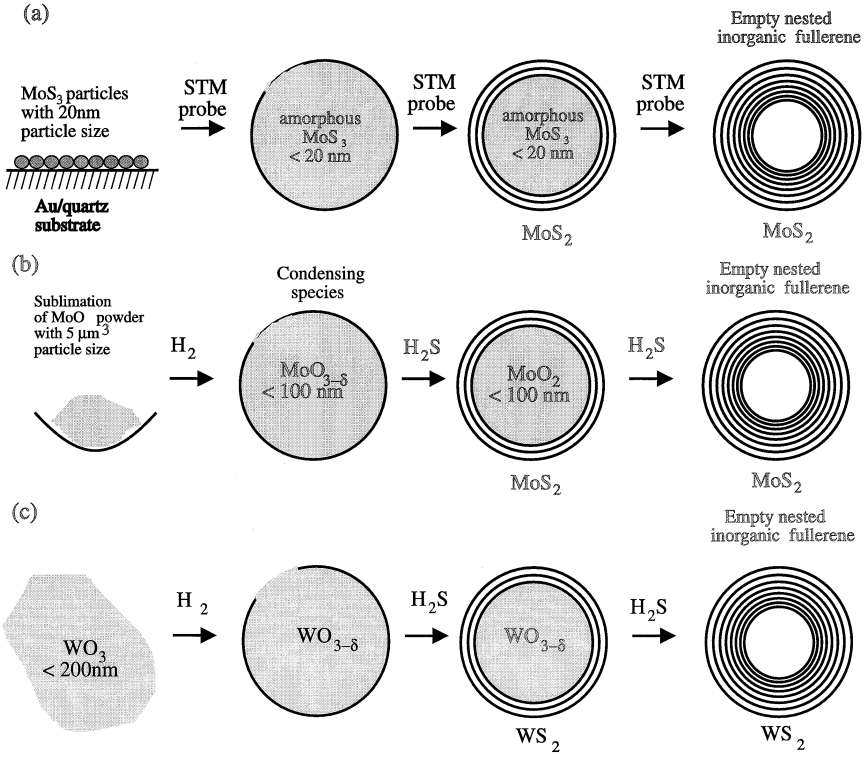

Fig. 8 Schemes showing: (a) mechanism of formation of MoS_2 induced by STM from MoS_3, resulting in the formation of amorphous MoS_3 encapsulates; (b) mechanism of gas-phase reaction of H_2S with MoO_{3-d} to form encapsulated oxide and empty MoS_2 inorganic fullerenes; (c) mechanism of gas–solid reaction of H_2S with solid WO_{3-d} to form encapsulated oxide and empty WS_2 inorganic fullerenes. All mechanisms eventually produce empty nested inorganic fullerenes (adapted from Feldman *et al.*[69]).

variety of products, from MoS_2 fullerenes, to MoS_2 nanotubes, to MoS_2 encapsulated MoO_{3-d}, obtained precisely by varying these conditions. In the case of the formation of WS_2 encapsulated WO_{3-d}, however, the situation is made more interesting by the fact that encapsulation occurs *via* reaction of H_2S gas with the reduced WO_3 solid in a situation analogous to the gas-phase carbon deposition onto solid catalytic particles, described above. Under these conditions, the overall morphology of the encapsulated species will be determined by the morphology of the reduced WO_{3-d} precursor particles. An example of this phenomenon is shown in the micrograph in Fig. 9(a). The encapsulate in this case is a 'bent' crystallite of WO_{3-d} encapsulated by a 'skin' of WS_2 fullerenic material. Closer inspection of the crystallite reveals that the bend in the crystallite is due to several grain boundaries (arrowed) that occur as defects within the crystal. A further interesting feature of these encapsulates is that, as partially reduced WO_3, there is always the potential that other types of defects and structural features may be observed inside encapsulates. This is in fact now the case.[70] In Fig. 9(b), an example of an encapsulated structure of the Wadsley defect type is shown. The shear planes observed in this encapsulate arise as a result of the corner-sharing WO_3 octahedra network partially collapsing to form shear planes comprised of edge-sharing WO_3 octahedra. A schematic representation of the encapsulated defect structure is shown in Fig. 9(c). Previously, this type of defect structure has only been observed in reduced single crystals of reduced WO_3.[71] Another new type of encapsulated structure is shown in Fig. 10. Inside a bilayer of WS_2 material, a novel layered tungsten oxide can clearly be seen. This is the first example of a complex layered structure formed inside a fullerene related structure. A more detailed analysis of the structure of this encapsulate will appear elsewhere.[70]

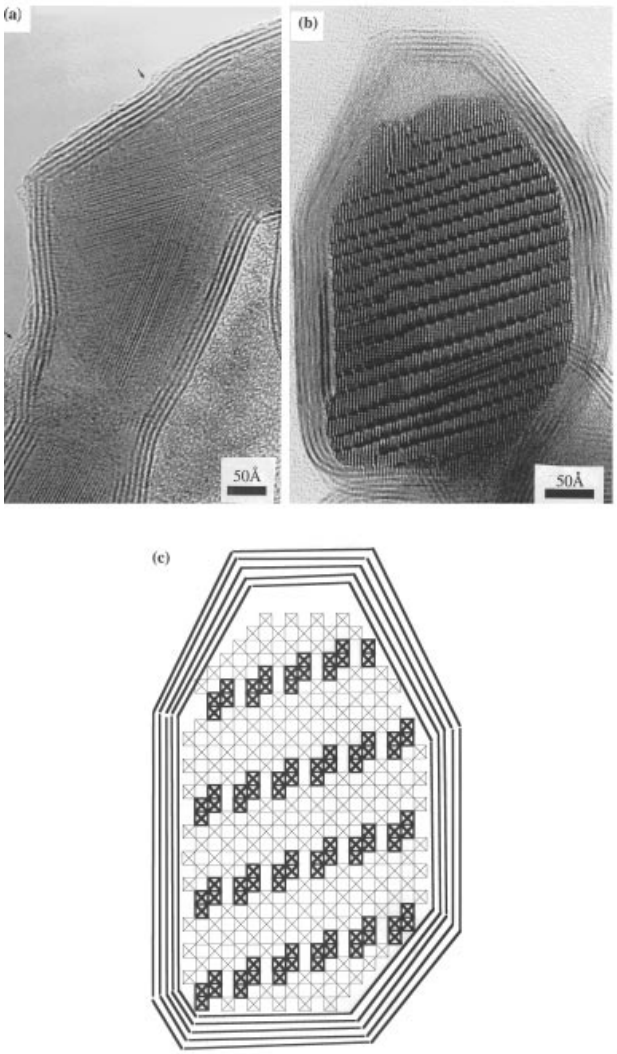

Fig. 9 (a) External morphology of encapsulate induced by defect structure of reduced oxide encapsulate. WS_2 skin follows the bend in the WO_{3-d} crystal induced by grain boundaries (arrowed). (b) Wadsley defect structure incorporated inside WS_2 nested fullerene. (c) Schematic representation of (b) showing how the partial collapse of WO_3 network leads to the formation of shear planes. The total number of shear planes depicted is 4, but there are no less than 18 inside the imaged structure.

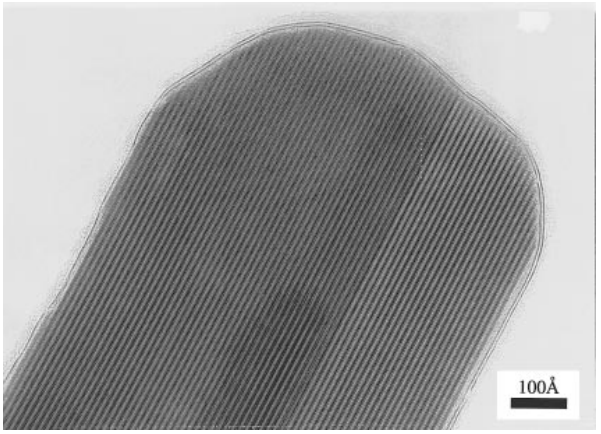

Fig. 10 Layered and lamellar reduced tungsten oxide structure observed inside WS_2 nested fullerene

Concluding remarks

The types of encapsulation behaviour discussed in this article raise the prospect of manipulating materials formation at the most intimate scale. The mechanisms of morphological control of nanotube capillaries over crystallite formation contribute to an understanding of how encapsulates such as nanowires can form inside nanotubes. The main benefit of catalytic encapsulation of materials, either *in situ* or by gas-phase deposition onto catalytic particles, is in the coating of reactive or air-sensitive species. In the case of *in situ* formed materials, an additional benefit lies in the fact that many of the encapsulated products are metastable and are often not readily obtainable by other methods. The observation of defect and layered materials inside inorganic fullerenes presents a wholly new perspective in encapsulation technology. These materials represent, for the first time, the first realistic possibility for incorporating complex layered or defect structures, with one or more useful properties, inside a wholly different type of structure, with completely different properties, thus generating a new class of hybrid materials.

The authors are indebted to Dr. Edman S. C. Tsang, of Reading University, for supplying the encapsulated MoO_3 specimen, to Dr. Jens Hammer and Rufus Heesom, of Oxford University, for preparing the encapsulated rhenium carbide specimen, to Dr. Andrew P. E. York, of the Inorganic Chemistry Laboratory, for the provision of the Ni-Harshaw specimen and also to Moshe Homyonfer and Yishai Feldman, of the Weizmann Institute, who prepared the WO_{3-d} encapsulated WS_2 specimen.

References

1 S. Iijima, *Nature* (*London*), 1991, **354**, 56.
2 P. M. Ajayan and S. Iijima, *Nature* (*London*), 1993, **361**, 333.
3 P. M. Ajayan, T. W. Ebbesen, T. Ichihashi, S. Iijima, K. Tanigaki and H. Hiura, *Nature* (*London*), 1993, **362**, 522.

4 S. C. Tsang, Y. K. Chen, P. J. F. Harris and M. L. H. Green, *Nature* (*London*), 1994, **372**, 159.
5 S. C. Tsang, J. J. Davis, M. L. H. Green, H. A. O. Hill, Y. C. Leung and P. J. Sadler, *J. Chem. Soc., Chem. Commun*., 1995, 2579.
6 S. Seraphin, D. Zhou, J. Jiao, J. C. Withers and R. Loufty, *Nature* (*London*), 1993, **362**, 503.
7 Y. Saito, T. Yoshikawa, M. Okuda, N. Fujimoto, K. Sumiyama, K. Suzuki, A. Kasuya and Y. Nishina, *J. Phys. Chem. Solids*, 1993, **54**, 1849.
8 D. Ugarte, *Chem. Phys. Lett*., 1993, **209**, 99.
9 P. M. Ajayan, C. Colliex, J. M. Lambert, P. Bernier, L. Barbedette, M. Tencé and O. Stephan, *Phys. Rev. Lett*., 1994, **72**, 1722.
10 S. Subramoney, R. S. Ruoff, D. C. Lorents, B. Chan, R. Malhorta, M. J. Dyer and K. Parvin, *Carbon*, 1994, **32**, 507.
11 C. Guerret-Piécourt, Y. Le Bouar, A. Loiseau and H. Pascard, *Nature* (*London*), 1994, **372**, 761.
12 J. W. Cowley and M. Liu, *Micron*, 1994, **25**, 53.
13 Y. Murakami, T. Shibata, K. Okuyama, T. Arai, H. Suematsu and Y. Yoshida, *J. Phys. Chem. Solids*, 1993, **54**, 1861.
14 A. Loiseau and H. Pascard, *Chem. Phys. Lett*., 1996, **256**, 246.
15 A. Loiseau, *Fullerene Sci. Technol*., 1996, **4**, 1263.
16 C. H. Kiang, W. A. Goddard, R. Beyers, J. R. Salem and D. S. Bethune, *J. Phys. Chem*., 1994, **98**, 6612.
17 S. Amelinckx, X. B. Zhang, D. Bernaerts, X. F. Zhang, V. Ivanov and J. B. Nagy, *Science*, 1994, **265**, 235.
18 D. Bernaerts, X. B. Zhang, X. F. Zhang, S. Amelinckx, G. Vantendeloo, J. Vanlanduyt, V. Ivanov and J. B. Nagy, *Philos. Mag. A*, 1995, **71**, 605.
19 Y. Saito, K. Nishikubo, K. Kawabata and T. Matsumoto, *J. Appl. Phys*., 1996, **80**, 3062.
20 R. Tenne, L. Margulis, M. Genut and G. Hodes, *Nature* (*London*), 1992, **360**, 444.
21 L. Margulis, G. Salitra and R. Tenne, *Nature* (*London*), 1992, **365**, 113.
22 M. Hershfinkel, L. A. Gheber, V. Volterra, J. L. Hutchison, L. Margulis and R. Tenne, *J. Am. Chem. Soc*., 1994, **116**, 1914.
23 L. Margulis, R. Tenne and S. Iijima, *Microsc. Microanal. Microstruct*., 1996, **7**, 87.
24 Y. Feldman, E. Wasserman, D. J. Srolovitz and R. Tenne, *Science*, 1995, **267**, 222.
25 S. C. Tsang, P. J. F. Harris and M. L. H. Green, *Nature* (*London*), 1993, **362**, 520.
26 Y. Yosida, *Appl. Phys. Lett*., 1994, **64**, 3048.
27 Y. Saito and M. Masuda, *Jpn. J. Appl. Phys., Part 1*, 1994, **34**, 5594.
28 J. Jiao, S. Seraphin, X. K. Wang and J. C. Withers, *J. Appl. Phys*., 1996, **80**, 103.
29 M. Freemantle, *Chem. Eng. News*, 1996, **74**, 62.
30 P. M. Ajayan, O. Stephan, P. Redlich and C. Colliex, *Nature* (*London*), 1995, **375**, 564.
31 S. M. Csicsery, *Stud. Surf. Sci. Catal*., 1995, **94**, 1.
32 R. Tenne, *Adv. Mater*., 1995, **7**, 965.
33 E. G. Bithell, A. Rawcliffe, S. C. Tsang, M. J. Goringe and M. L. H. Green, *Inst. Phys. Conf. Ser*., 1995, **147**, 361.
34 J. Cook, J. Sloan, A. Chu, M. Zwiefka-Sibley, M. L. H. Green and J. L. Hutchison, *J. Solid State Chem*., submitted.
35 J. Sloan, J. Cook, R. Heesom, M. L. H. Green and J. L. Hutchison, *J. Cryst. Growth*, 1997, in press.
36 F. Banhart and P. M. Ajayan, *Nature* (*London*), 1996, **382**, 433.
37 R. M. Lago, S. C. Tsang, K. L. Lu, Y. K. Chen and M. L. H. Green, *J. Chem. Soc., Chem. Commun*., 1995, 1355.
38 Y. K. Chen, A. Chu, J. Cook, M. L. H. Green, P. J. F. Harris, R. Heesom, M. Humphries, J. Sloan, S. C. Tsang and J. C. F. Turner, *J. Mater. Chem*., 1997, in press.
39 A. Chu, J. Cook, R. Heesom, J. L. Hutchison, M. L. H. Green and J. Sloan, *Chem. Mater*., 1996, in press.
40 Y. K. Chen, M. L. H. Green and S. C. Tsang, *Chem. Commun*., 1996, 2489.
41 Y. Yosida, S. Shida, T. Oshuna and N. Shiraga, *Abstr. Fall Meeting Phys. Soc. Jpn*., 1993, **2**, 414.
42 M. Tomita, Y. Saito and T. Hayashi, *Jpn. J. Appl. Phys*., 1993, **32**, L280.
43 M. Ata, Y. Kijima, A. J. Hudson, H. Imoto, N. Matsuzawa and N. Takahashi, *Adv. Mater*., 1994, **6**, 590.
44 T. Hayashi, S. Hirono, M. Tomita and S. Umemura, *Nature* (*London*), 1996, **372**, 772.
45 S. Seraphin, D. Zhou and J. Jiao, *J. Appl. Phys*., 1996, **381**, 772.
46 N. S. Kopelev, V. Chechersky, A. Nath, Z. L. Wang, E. Kuzmann, B. S. Zhang and G. H. Via, *Chem. Mater*., 1995, **7**, 1419.
47 M. G. Liu and J. M. Cowley, *Carbon*, 1995, **33**, 749.
48 J. P. Hare, W. K. Hsu, H. W. Kroto, A. Lappas, K. Prassides, M. Terrones and D. R. M. Walton, *Chem. Mater*., 1996, **8**, 6.
49 S. Bandow and Y. Saito, *Jpn. J. Appl. Phys*., 1993, **32**, L1677.
50 Y. Wang, *J. Am. Chem. Soc*., 1994, **116**, 397.
51 J. Sloan, J. Cook, J. Hammer, R. Heesom and M. L. H. Green, in preparation.
52 H. Funasaka, K. Sugiyama, K. Yamamoto and T. Takahashi, *J. Appl. Phys*., 1995, **78**, 5320.
53 J. R. Rostrup-Nielsen, *Catal. Sci. Technol*., 1984, **5**, 1.
54 R. Lamber, N. Jaeger and G. Schulz-Ekloff, *Surf. Sci*., 1988, **197**, 402.
55 S. C. Tsang, J. B. Claridge and M. L. H. Green, *Catal. Today*, 1995, **23**, 3.
56 P. E. Nolan, D. C. Lynch and A. H. Cutler, *Carbon*, 1996, **34**, 817.
57 S. Motojima, S. Asakura and M. Hirata, *Mater. Sci. Eng. B*, 1995, **34**, L9.
58 M. Endo, K. Takeuchi, K. Kobori, K. Takahashi, H. W. Kroto and A. Sarkar, *Carbon*, 1995, **33**, 873.
59 N. A. Kiselev, J. Sloan, D. N. Zakharov, E. F. Kukovitskii, J. L. Hutchison, J. Hammer and A. S. Kotosonov, in preparation.
60 M. Yudasaka, R. Kikuchi, T. Matsui, Y. Ohki, S. Yoshimura and E. Ota, *Appl. Phys. Lett*., 1995, **67**, 2477.
61 J. Y. Dai, J. M. Lauerhaas, A. A. Setlur and R. P. H. Chang, *Chem. Phys. Lett*., 1996, **258**, 547.
62 L. Margulis, J. L. Hutchison and R. Tenne, in *New Horizons for Materials*, ed. P. Vincenzini, Techna Sci, Italy, 1995, pp. 301–308.
63 M. S. Donley, N. T. McDevitt, T. W. Hass, P. T. Murray and J. T. Grant, *Thin Solid Films*, 1989, **168**, 335.
64 Q. Zhang, R. B. Huang, Z. Y. Liu and L. S. Zheng, *Chem. J. Chin. Univ*., 1995, **16**, 1624.
65 M. Homyonfer, Y. Matsai, M. Hershfinkel, V. Volterra, J. L. Hutchison and R. Tenne, *J. Am. Chem. Soc*., 1996, **118**, 7804.
66 R. Heesom, Part II Thesis, Oxford, 1996.
67 Y. Saito, M. Okuda, T. Yoshikawa, A. Kasuya and Y. Nishina, *J. Phys. Chem*., 1994, **98**, 6696.
68 R. Lamber, N. Jaeger and G. Schulz-Ekloff, *Surf. Sci*., 1988, **197**, 402.
69 Y. Feldman, G. L. Frey, M. Homyonfer, V. Lyakhovitskaya, L. Margulis, H. Cohen, G. Hodes, J. L. Hutchison and R. Tenne, *J. Am. Chem. Soc*., 1996, **118**, 5362.
70 J. Sloan, J. L. Hutchison, R. Tenne, M. Homyonfer, Y. Feldman and T. Tsirlana, in preparation.
71 R. J. D. Tilley, *Chem. Scr*., 1979, **14**, 147.

Paper 7/00035I; *Received* 2*nd January*, 1997